Optimisation of pack chromised stainless steel for proton exchange membrane fuel cells bipolar plates using response surface methodology

Olabi, Abdul-Ghani; Benyounis, Khaled; Stokes, Joseph; Oladoye, Atinuke; Carton, James

Published in:
Surface & Coatings Technology

DOI:
10.1016/j.surfcoat.2016.07.023

Published: 25/10/2016

Document Version
Peer reviewed version

Optimisation of pack chromised stainless steel for proton exchange membrane fuel cells bipolar plates using response surface methodology

A.M. Oladoye[1*], J. G. Carton[1], K. Benyounis[1], J. Stokes[1] and A. G. Olabi[2]

[1]School of Mechanical and Manufacturing Engineering, Dublin City University, Ireland

[2]University of the West of Scotland, Paisley, United Kingdom.

*Corresponding author: atinuke.oladoye2@mail.dcu.ie, +353899855456

Abstract

Stainless steels, as low cost materials, are attractive for Proton exchange membrane fuel cells (PEMFC) bipolar plates. However, these alloys require surface coatings or treatments to enhance its corrosion resistance and surface conductivity in PEMFC environments. In this study, response surface methodology based on Box–Behnken design was employed to investigate the influence of activator content, time and temperature on corrosion current density of chromised 304 stainless steel in simulated PEMFC environment of aerated 0.5M H_2SO_4 + 2 ppm HF at 70^oC. These process parameters were optimised and the performance of the optimised coatings in simulated and real PEMFC environments was investigated. The results indicated that temperature was the most significant factor influencing the performance of chromised coatings in PEMFC environments. The optimised coating produced at 1040^oC for 3 hours with powder containing 6.84 wt% activator content exhibited better corrosion resistance than the substrate in typical PEMFC cathode and anode environments respectively as well as about six fold decrease in the contact resistance of the substrate at 150 N/cm^2. Hence, the single fuel cell assembled with the bipolar plate coated with the optimised process

parameters exhibited a two-fold increase in the maximum power density of the cell with the uncoated bipolar plates.

Keywords: Chromised coatings, 304 stainless steel, Box-Behnken Design, Corrosion resistance, Bipolar plate.

1.0 INTRODUCTION

Rising energy and environmental concerns on the use of petroleum based fuels in automobiles and other transportation devices have generated global research interest in hydrogen fuelled proton exchange membrane fuel cells (PEMFC) as alternative power sources for such systems. Nevertheless, PEMFC are expensive and not as durable as conventional power sources despite its high power density, low operating temperature (60–80^{o}C) and near zero emissions advantages [1-4]. Hence, extensive research efforts have been directed toward cost reduction of PEMFC major components such as the bipolar plates.

A typical PEMFC stack consists of multiple single fuel cells arranged in series with each cell made up of a membrane electrode assembly sandwiched between two bipolar plates thereby making the latter the most repeated stack component. Hence, the bipolar plates account for a significant proportion of the cost, weight and volume of the stack. These plates also perform core functions such as distribution of reactant gases over the active electrode area and removal of water and heat within the cells that govern the power output and durability of the PEMFC stack. Bipolar plates are traditionally fabricated from non-porous graphite due to its corrosion resistance and high surface conductivity but its high gas permeability, brittleness and high processing cost are of major concern. Thus, alternative materials such as stainless steel alloys which offer lighter weight, higher mechanical strength and lower production cost

advantages over graphite have been considered as potential replacement for graphite [4-7]. These ferrous based alloys are, however, prone to corrosion in the humid and acidic PEMFC environments and exhibit high contact resistance with the gas diffusion layer (GDL) resulting in performance degradation of the PEMFC stack.

Surface modification of stainless steels via coatings and surface treatments have been widely adopted as means of enhancing its corrosion resistance and surface conductivity in PEMFC environments. Accordingly, the performance of several types of coatings and treatments, which are basically grouped into metal based- and carbon based coatings have been reported [3, 6, 8-15]. Among the coatings investigated, chromised coatings produced via pack cementation are a class of low cost diffusion coatings reported to enhance the performance of stainless steels in PEMFC environments [11-15]. Pioneering investigations on the application of chromised coatings for PEMFC bipolar plate application was reported by Cho et al. [11, 12]. In their first paper, the authors reported the influence of chromising time (2.5, 5 and 10 hours) on the corrosion of chromised 316 stainless steels produced at 1100^{o}C in a simulated PEM fuel cell environment of 1M H_2SO_4 at 80^{o}C. The results indicated that extended chromising time (10 hours) degraded the performance of the coatings in simulated PEMFC cathodic environment and working potentials. The second paper described the effect of heat-treatment time (2.5 hours and 23 hours) and powder composition on chromised 316 stainless steel produced at 1050^{o}C. Their results indicated that the phases formed during chromising, which dictated the surface conductivity of the chromised coating, were dependent on the process parameters investigated. In a third paper, the authors reported further attempts to improve the performance of chromised coatings via shot peening prior to chromising at 900^{o}C [13]. The improvement in corrosion behaviour was attributed to a thicker chromised

layer of pre-treated 316L stainless steel due to increased grain boundary densities during shot peening which facilitated higher diffusion of Cr at chromising temperatures. Wen et al. [14] investigated the effect of rolling pre-treatments and EDM machining coupled with low temperature chromising at 700^{o}C on 420 stainless steel and reported that rolling pre-treatments was more effective in enhancing the performance of chromised 420 stainless steel than EDM machining. Bai et al. [15] also reported that rolling pre-treatments improved the single fuel cell performance of low temperature chromised 316, 430 and 420 stainless steels. These studies evidently showed that the performance of chromised coatings in PEMFC environments depended on the substrate composition and process parameters. Nonetheless, only a few stainless steel alloys and process parameters have been investigated.

Furthermore, Cho et al [11, 12] in their first two papers reported optimum conditions for obtaining best corrosion resistance at 1050^{o}C and 1100^{o}C respectively within very limited range of parameters. However, it is important to fully understand the complete effect of process parameters (time, temperature, powder composition) on the corrosion resistance of chromised stainless steels in PEMFC in order to establish optimum process conditions. Also, the classical experimental approach of one-facto-at-a-time employed in these studies may not be able to establish an accurate optimum point as well as indicate possible interaction between the process parameters. Hence, in this study, design of experiments technique named response surface methodology (RSM) was utilised to systemically investigate the influence of time, temperature and activator content on corrosion performance of chromised stainless steels in simulated PEMFC environments and optimise the selected process parameters.

The present study also investigated the single fuel cell performance of the chromised stainless steel produced at optimum process parameters in order to evaluate the suitability of chromised coating produced without pre-treatments for PEMFC bipolar plates as only ex-situ performance of these coatings have been reported in the literature.

2.0 Experimental Procedure

2.1 Response surface design

RSM consists of a collection of mathematical and statistical tools used for designing experiments, developing empirical models and optimising process output(s) influenced by many factors [16-18]. In contrast to classical experimental method employed in previous studies on chromised stainless steels for bipolar application [11-15], RSM can establish optimal process parameters with fewer experiments and also deduce interactive effects between process parameters if any. Box–Behnken design, one of the basic RSM models consisting of rotatable or nearly rotatable three-level second-order designs based on incomplete factorial designs [4,16], was utilised to develop the design matrix which consisted of seven experiments with five centre points and two replicates. Three-levels were chosen for the selected process parameters: time activator content (B), temperature (C) as given in Table 1 while the design matrix and experimental results are given in Table 2. The process parameters and the values shown in Table 1 were selected based on the literature on chromised coatings without pre-treatments [11, 12, 19-21]. The Experimental result in Table 2 was fitted into a second-order polynomial model given in Equ.1 as suggested by the model summary statistics presented in Appendix A.

$$Y = \beta_o + \sum_{i=1}^{3} \beta_o x_i + \sum_{i=1}^{3} \beta_{ii} x_i^2 + \sum_{i=1}^{3} \sum_{i<j}^{3} \beta_{ij} x_i x_j + \varepsilon \qquad Equ. 1$$

where Y is the predicted response, β_o is the coefficient of intercept, βi is the coefficient of linear effect, βii is the coefficient of quadratic effect, βij, is the coefficient of interaction effect, i and j are index numbers for the independent variables and ε is the random error.

The adequacy of the model was evaluated using Analysis of variance (ANOVA) and analysis of the residuals. Design Expert statistical software package version 9.0.2.0 (State-Ease Inc., USA) was employed for designing the experiments and analysing the experimental data as well as generating the response surface plots and optimising the process parameters.

2.2 Materials

Commercially available, 2mm thick, 304 stainless steel coupons (Impact Metals Ireland, Dublin) with nominal composition of Fe-18Cr-10Ni-2Mn-1Si-0.08C all in wt% were ground with silicon carbide papers, ultrasonically cleansed in acetone and air-dried prior to pack cementation. The coupons were thereafter embedded in a previously ball-milled powder pack composed of 50 wt. % Cr powder, (B) wt. % of NH_4Cl and (50-B) wt. % of alumina where the value of B is as shown in Table 1. The crucibles were sealed with fire clay, cured in an oven to solidify the clay and afterwards loaded into a tube furnace with argon gas protection. Pack cementation of the stainless steel samples was conducted randomly as specified in the design matrix. After the heat treatment cycle, the chromised stainless steel samples were cleansed in acetone and dried in air.

2.3 Surface Characterisation

Surface morphologies and thickness of the chromised stainless steels was characterised with a ZEISS EVO LS15 Scanning electron Microscope (SEM) equipped with INCA Energy dispersive X-ray (EDX) spectrometer (Oxford instruments). Phase analysis of the coatings produced at the optimised process parameters was accomplished with a D8 Advance Buker XRD with Cu Kα radiation (λ= 0.154nm) and operated at 40 KV and 40 mA. XPS spectra the optimised coatings were obtained with a Kratos Axis Ultra XPS model with Al X-ray source (1486.6 eV) at Nano Imaging and Material Analysis Centre, Ireland. XPS spectra were referenced to adventitious C1s at 284.5 eV and obtained at constant pass energy of 20 eV and 0.05 stepwise before and after argon ion sputtering.

2.4 Electrochemical experiments

Electrochemical polarisation experiments were conducted via conventional three electrode system consisting of Ag/AgCl (saturated KCl) as reference electrode, platinum mesh as the counter electrode and the chromised stainless steel samples as the working electrode. All experiments were conducted in a flat cell exposing $1cm^2$ of the working electrode to the electrolyte, 0.5 M H_2SO_4 + 2 ppm HF at 70^oC. The samples were soaked in the electrolyte for 180 minutes and open circuit potential (OCP) was measured till the system was stable, Tafel polarisation was thereafter conducted at ± 0.3 V vs (OCP) at a scanning rate of 1 mV/s using CHI 630C potentiostat (CH Instruments, USA). Tafel polarisation experiments were conducted with two samples and average values of corrosion current densities obtained by using Tafel analysis in the CHI software are reported in Table 2. Potentiodynamic polarisation of the optimised coating was conducted with Gamry Interface 1000™ potentiostat/galvanostat at a scanning rate of 1 mV/s from -0.1V vs OCP to 1.2 V vs.

Reference. The experiments were repeated three times with hydrogen gas and air bubbled into the electrolyte during polarisation to depict PEMFC anodic and cathodic environments respectively.

2.5 Interfacial contact resistance

Interfacial contact resistance (ICR) between carbon paper and the sample was evaluated at room temperature as described by Wang et al. [9]. In summary, experimental set up for the measurement consisted of two of pieces of Toray Teflon treated carbon paper (20% PTFE, TGP-H-90, Fuel cell Earth, USA) sandwiched between the optimised chromised sample and two copper electrodes. A direct current of 1 A was supplied to the copper electrodes via a XHR 300-3.5DC power source. The voltage drop across the setup was measured with Tektronix DMM912 digital multi-meter while the compaction force was gradually applied by a Zwick Roell universal testing machine.

2.6 Single fuel cell test

Single fuel cells were assembled with 304 stainless steel bipolar plates coated and uncoated with the optimised process parameters fabricated in-house. Pictures of the bipolar plates and single cells can be found in Appendix B. Each cell had an active area of $5cm^2$ with 35mm x 35mm x 2mm bipolar plates with serpentine flow designs and commercially available coated membrane and GDL (Fuel cell stores, USA). The cells were purged with nitrogen gas before operating the cells at room temperature. Humidified hydrogen gas and compressed air were thereafter supplied to the cell at 50 ml/min after which the performance of the cells was evaluated in terms of cell voltage and power densities as a function of current density.

3.0 Result and Discussion

3.1.1 Regression Analysis and ANOVA

Regression analysis and ANOVA was used to evaluate the significance of the response surface model and the influence of the process parameters on corrosion current density. Regression analysis indicated that the model showed a good degree of fitness with a coefficient of determination (R^2) of 0.9401 implying that the model can account for 94.01% of the variation in the data. The adjusted R^2 and predicted R^2 for the model also showed good correlation with values of close to 1 (Table 3). The ANOVA result presented in Table 3 indicated that the model was statistically significant at 95% confidence level with F-value of 34.50 and p-value < 0.0001. The significant model terms in descending order were: second order term of temperature (C^2) > interaction between temperature and activator content (BC) > time (A) > linear term of temperature (C). The analysis of residuals also indicated the model assumption of normality was satisfied, hence, the model can make adequate prediction (Plots can be found in Appendix C).

The best model describing the relationship between the response and the process parameters was obtained after square root transformation and is given in Equ. 2.

$$(y)^{0.5} = +0.473 + 1.280\,x\,10^{-4} * A - 6.402\,x\,10^{-3} * B - 8.648\,x\,10^{-4} * C + 6.0373\,x\,10^{-6} * BC + 3.950\,x\,10^{-7} * C^2 \qquad Equ.2$$

Where y is the corrosion current density and A, B, C are given as time in hours, activator content in wt. % and temperature in ^{o}C respectively. Equ. 2 is consistent with the ANOVA result indicating that the second order term of temperature had the most significant influence

on the corrosion current density of chromised 304 stainless steel in 0.5M H_2SO_4 + 2 ppm HF at 70^oC.

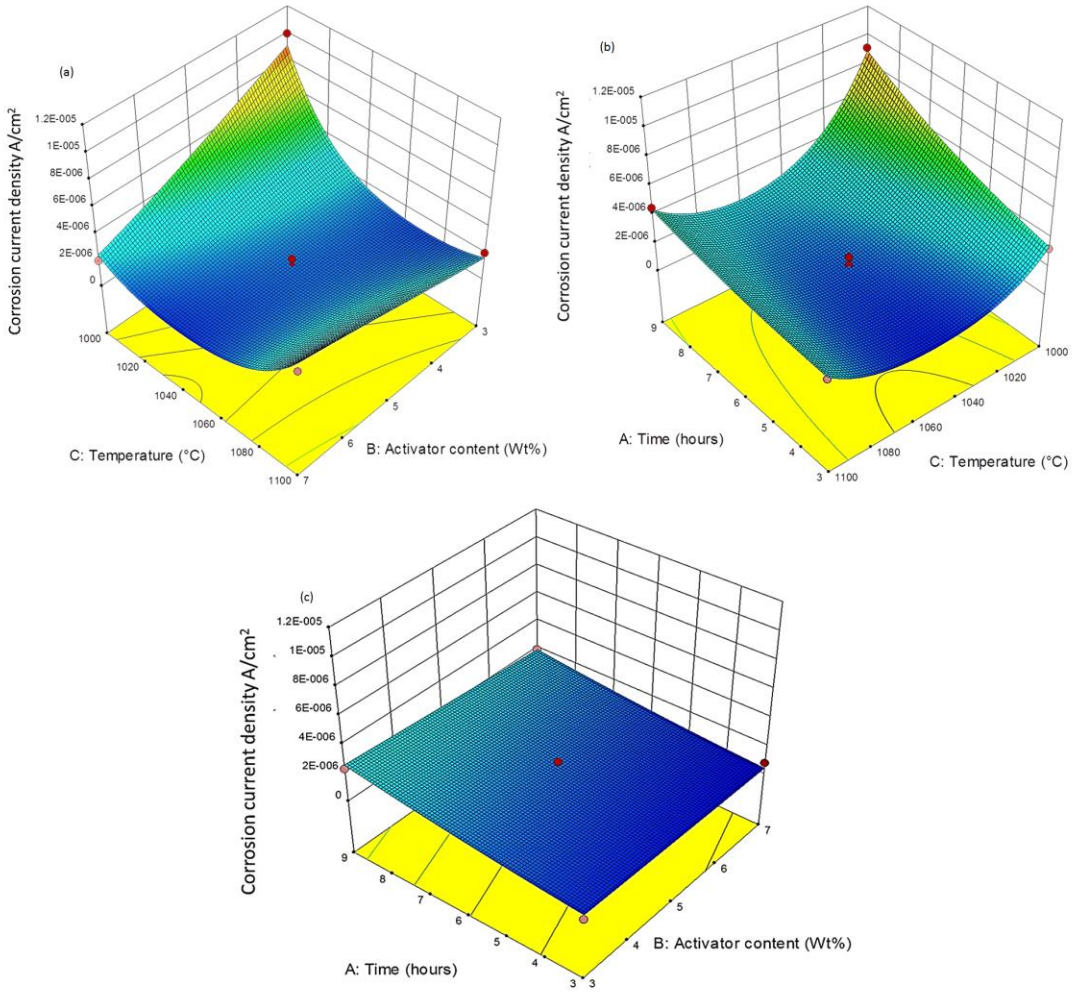

Fig. 1 Surface plots (a) temperature vs. activator content, (b) time vs temperature, (c) time vs. temperature

3.1.2 Influence of process parameters on corrosion current density of chromised stainless steels in 0.5M H_2SO_4 + 2 ppm HF.

Fig. 1 shows the response surface plots of the mutual interaction between corrosion density and the process parameters: time , activator content (B), temperature (C) It can be seen from the response surface plots in Fig. 1a and b that at constant activator content and time, corrosion current density decreased parabolically as the temperature increased from 1000^{o}C to 1100^{o}C. For instance, at constant activator content of 3 wt. % and time of 6 hours , corrosion current density of chromised stainless steel produced at 1000^{o}C (R6 in Table 2) was 1.00 x 10^{-5} A/cm^{2} , however, when temperature increased to 1100^{o}C, corrosion current density decreased to 2.05 x 10^{-6} A/cm^{2} (R1 in Table 2). Examination of the surface morphologies of samples R6 and R1 shown in Fig. 2a, & b indicate significant changes in the morphologies of the coatings as temperature increased. At 1000^{o}C, a porous network-like structure matrix with small sized clusters is formed as shown in Fig. 2a, The inset of Fig. 2a shows the porous matrix of R6 at a higher magnification. This porous matrix will facilitate electrolyte-substrate interaction thereby deteriorating the corrosion resistance of R1 [22]. However, as temperature increased to 1100^{o}C, a compact surface with bigger-sized clusters and large grain size of network carbide which can provide better corrosion resistance than a porous coating was formed.

The influence of time on corrosion current density is presented in Fig. 1 b and c. It can be seen from these surface plots that corrosion current density increased linearly with time. Although longer duration of chromising treatment can facilitate higher coating thickness at constant temperature and activator content as seen in the case of samples R12 and R17, R13 and R16 as well as R4 and R5. Nevertheless, as time increased from 3 hours to 9 hours, the coating formed is more susceptible to defects such as voids and pores arising from the difference in the inward diffusion rate of chromium and outward diffusion rate of carbon

[23]. An example of such effect can be seen in the surface morphologies of R13 and R16 (Figure 2c and d) produced at temperature of 1050^{o}C and activator content of 7 wt. % for 3 and 9 hours respectively wherein an order of magnitude increase was observed in R16 compared to R13 as time increased.

Fig. 1a and c depicts the influence of activator content on corrosion current density. Combining the response surface plots and the ANOVA results, it can be seen that the effect of the activator content on corrosion current density was considerably low at constant temperature and time. An illustration of this effect can be seen in the corrosion density of samples R16 and R17 pack cemented at 1100^{o}C for 9 hours with powder containing 3 wt. % and 7 wt % of activator content respectively. The corrosion current density for R16 was found to be 1.889 A/cm^2 while that of R17 was 2.345 A/cm^2. Examination of the surface morphologies of these samples shown in in Fig. 2d and e suggest that the similarity in corrosion performance of these coatings could be attributed to the similarity in surface morphologies.

3.1.3 Optimisation of process parameters

Optimisation of process parameters was conducted using numerical simulation coupled with the desirability function using the conditions shown in Table 4. The method adopted determines the optimum condition by first locating the level of each factor that can achieve the predicted response after which the overall desirability is maximised based on the set goals [16]. A set of solution with desirability value of 1 and similar corrosion current densities was obtained, however, the condition selected by the software was: activator content of 6.84 wt. %, time of 3.04 hours and temperature of 1040^{o}C, with a predicted corrosion density value of 3.895 x 10^{-7} A/cm^2. Experiments to verify the optimal conditions were conducted with three

samples and average corrosion current density of 4.304 (± 0.73) x 10^{-7} A/cm^2 was obtained when the coatings was polarised in aerated 0.5M H_2SO_4 + 2 ppm HF at 70^oC.

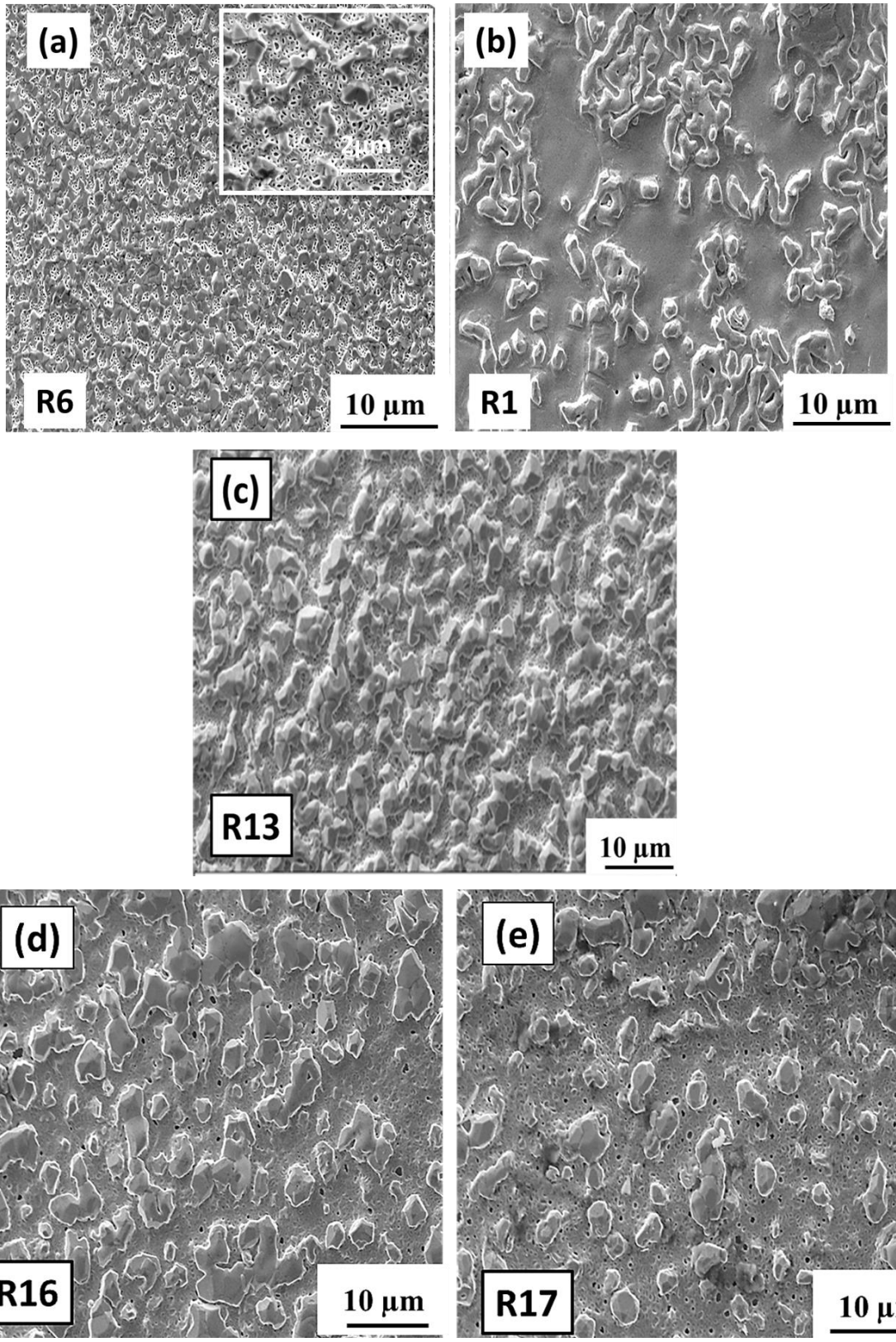
(a)
2 µm
R6
10 µm
(b)
R1
10 µm
(c)
R13
10 µm
(d)
R16
10 µm
(e)
R17
10 µm

Fig. 2: SEM images of chromised stainless steel sample (a) R6, (b) R1 (c) R13 (d) R 16 (e) R17

3.2 Chromised 304 stainless steel produced at optimal process conditions

3.2.1 Surface Characterisation

Fig. 3 displays the surface morphology and cross sectional view of the chromised stainless steel produced at the optimised process parameters, hereafter, named Cr-304. The SEM image revealed a coarse and granular surface morphology. The thickness of the optimised coating was estimated to ~30µm using EDX line scan. EDX analysis of the optimised surface indicated that the chromised surface consisted primarily of chromium (67.12 at. %), carbon (9.46 at. %) and nitrogen (18.30 at. %) with minor amount of oxygen (2.34 at. %) and iron (2.25 at. %) as well as trace amount of aluminium which originated from the alumina in the powder pack.

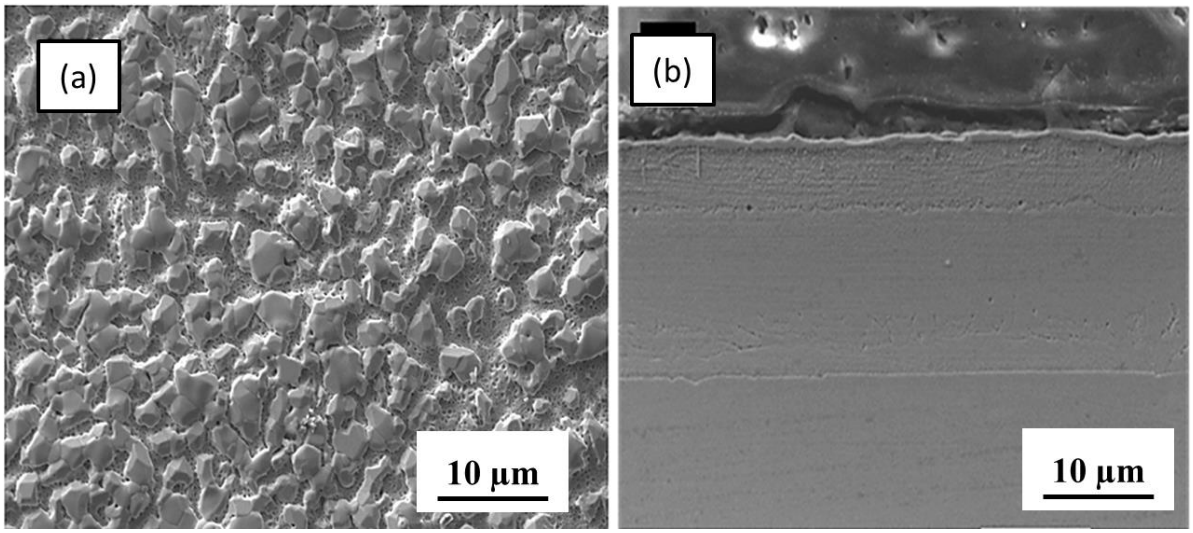

Fig. 3: (a) Surface morphology and (b) Cross-sectional view of Cr-304

The XPS survey spectra of the optimised surface presented in Fig. 4a is consistent with the EDX analysis but shows no Fe2p peak signifying minimal concentration of Fe on the superficial layer in agreement with previous investigation on chromised 304 type stainless steel produced by fluidised bed CVD [21]. The Cr2p narrow scan region (Fig. 4b) established the presence of chromium carbide at a binding energy of 540.0 eV [24, 25], chromium nitride in oxygen environment at a binding energy of 575.5 eV [26, 27] and chromium oxide at a binding energy of 577.0 eV [26, 27].

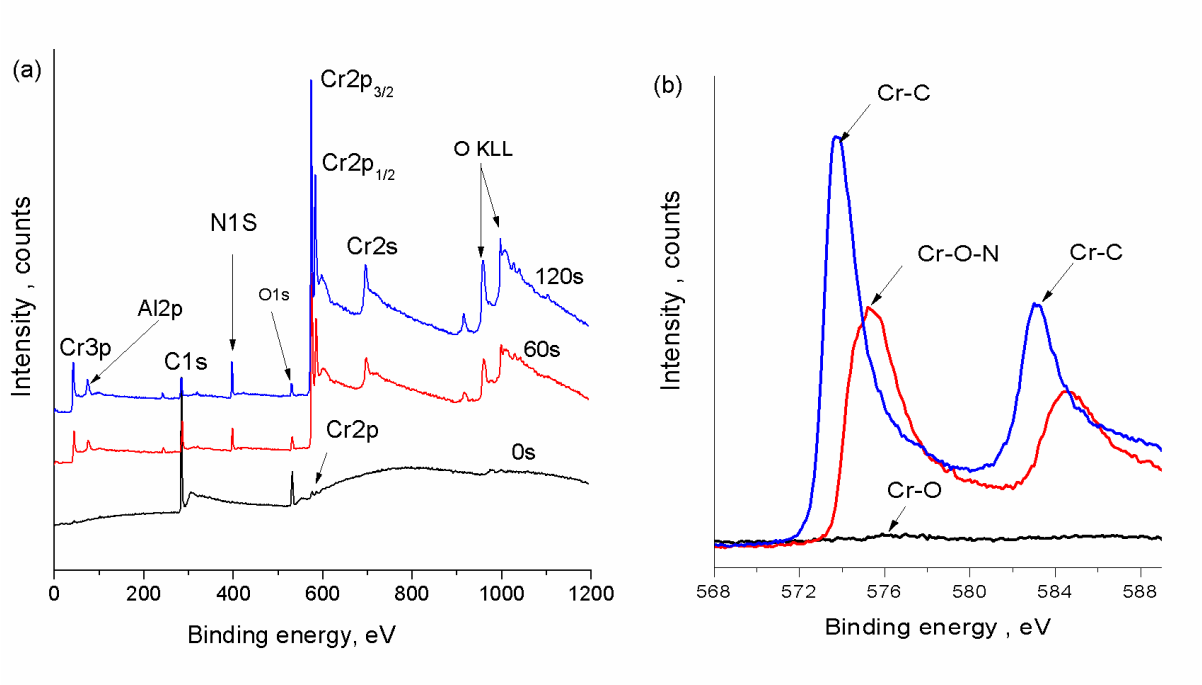

Fig. 4: XPS analysis of Cr-304 (a) survey spectrum (b) narrow region scan for Cr2p

Glancing XRD patterns for Cr-304 (Fig. 5) further confirmed the presence of the chromium based compounds identified in Fig. 4b on the near surface of Cr-304 with diffraction peaks attributed to $(Cr,Fe)_{23}C_6$, $(Cr, Fe)_3C_7$ and $(Cr, Fe)_2N_{1-x}$ phases. GXRD, however, did not

detected chromium oxide, which is attributed to surface oxidation, due to its low concentrations compared to the other compounds.

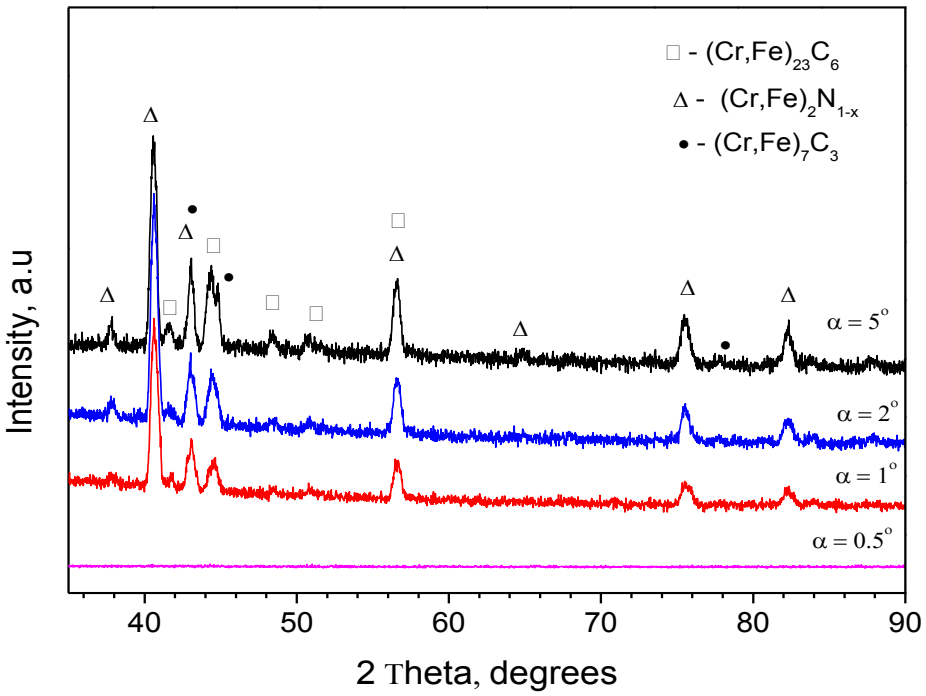

Fig. 5: Glancing incidence angle XRD of Cr-304

3.2.2 Electrochemical Polarisation

Fig 6a and b presents typical dynamic polarisation curves obtained for Cr-304 and the substrate (SS304) in 0.5 M H_2SO_4 + 2 ppm HF at 70°C with air and hydrogen gas bubbling environments to depict PEMFC cathode and anode environments respectively. In both environments as shown in Table 5, Cr-304 exhibited more noble potential and reduced corrosion current density than the substrate indicating that chromising treatments improved the corrosion properties of the substrate. This observation is consistent with previous studies on chromised stainless steels [11-15]. In the simulated cathode environment (Fig 6a), both Cr-304 and SS304 exhibited similar passive–transpassive behaviours achieving trans-passivation at ~ 0.9V. It can also be seen from Fig. 6a that both materials are within the

passive region at PEMFC cathode potential of 0.6 V. On the other hand, in the anode environment (Fig. 6b), the open circuit potential of Cr-304 is close to the anode PEMFC

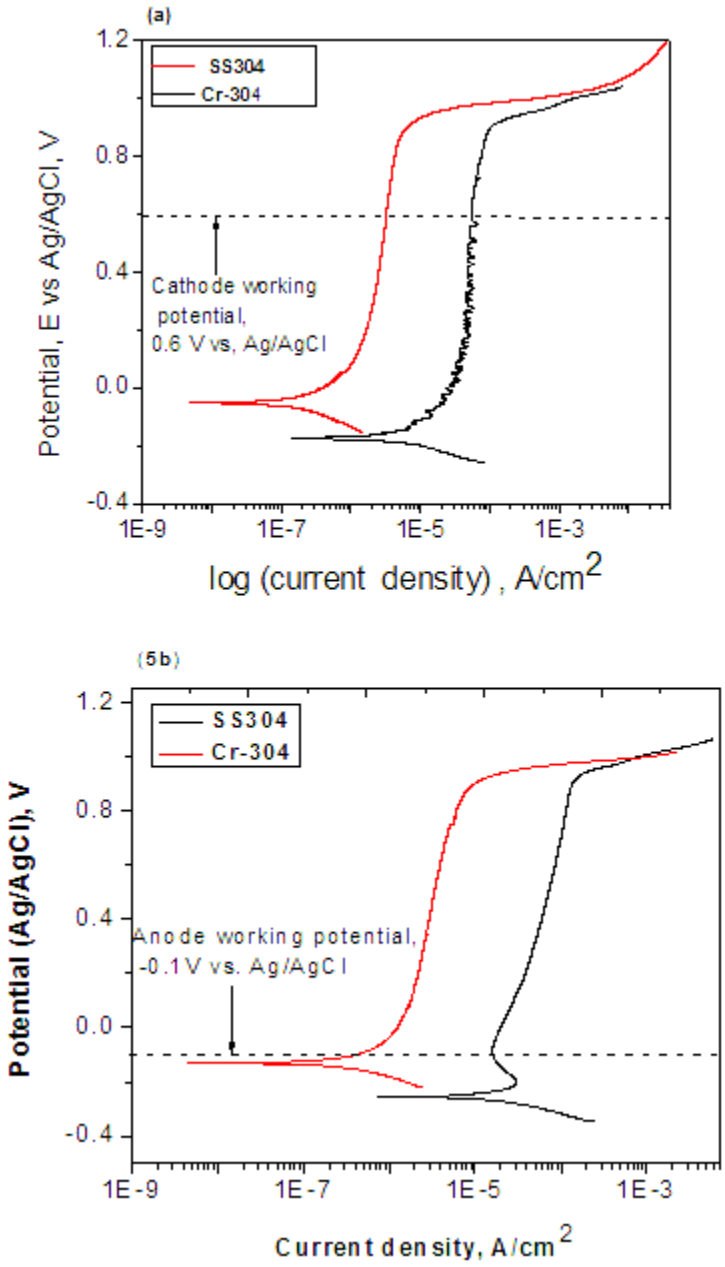

Fig. 6: Dynamic polarisation curves for Cr-304 and SS304 in simulated PEMFC (a) cathodic (b) anodic environments

working potential while SS304 is still within the passive region in simulated anode environment. Furthermore, in the anode environment, SS304 exhibited an active region of dissolution with a passivation current of -25.9 μA/cm^2 after which it experienced similar passivity with Cr-304 within a potential range of ~ -0.1 V to +0.9 V. The improvement in corrosion behaviour of Cr-304 compared to that of SS304 in both oxidising and reducing environments can be attributed to the presence of chromium nitrides and carbides on the near-surface of Cr-304 as seen in the XPS and GXRD analysis.

3.3.3 ICR and single fuel cell performance.

Fig. 7a is the plot of ICR as a function of compaction pressure for Cr-304 and SS304. It can be seen that ICR decreased as compaction pressure increased due to increasing contact area between the carbon paper and the metal samples. Cr-304 exhibited an order of magnitude decrease in ICR compared to SS304 within the range of compacting pressure investigated signifying the beneficial effect of chromising on the surface conductivity of 304 stainless steel. At the compaction pressure range of interest for PEMFC applications (i.e. 100 - 200N/cm^2 [3, 6]), SS304 exhibited ICR values between 195.7 to 114.9 mΩ/cm^2 while Cr-304 exhibited ICR values between 35.10 to 19.00 mΩ/cm^2. At typical PEM fuel cell compaction force of 150N/cm^2, Cr-304 exhibited ICR value of 24 mΩ.cm^2 while that of the substrate was 143.29 mΩ/cm^2.

Notably, the ICR values of Cr-304 and SS304 are higher than ICR values reported in the literature for bare 304 stainless steels and chromised stainless steels [10-15, 28]. The higher ICR value for both materials is attributed to the PTFE loading of the carbon paper employed for ICR measurement. It is reported that the contact resistance of bipolar plate materials increases with increase in the PTFE loading of the carbon paper or GDL material [29, 30]. It

is also noted that the PTFE loading of the carbon paper used for ICR measurements in previous studies on chromised stainless steels were unreported.

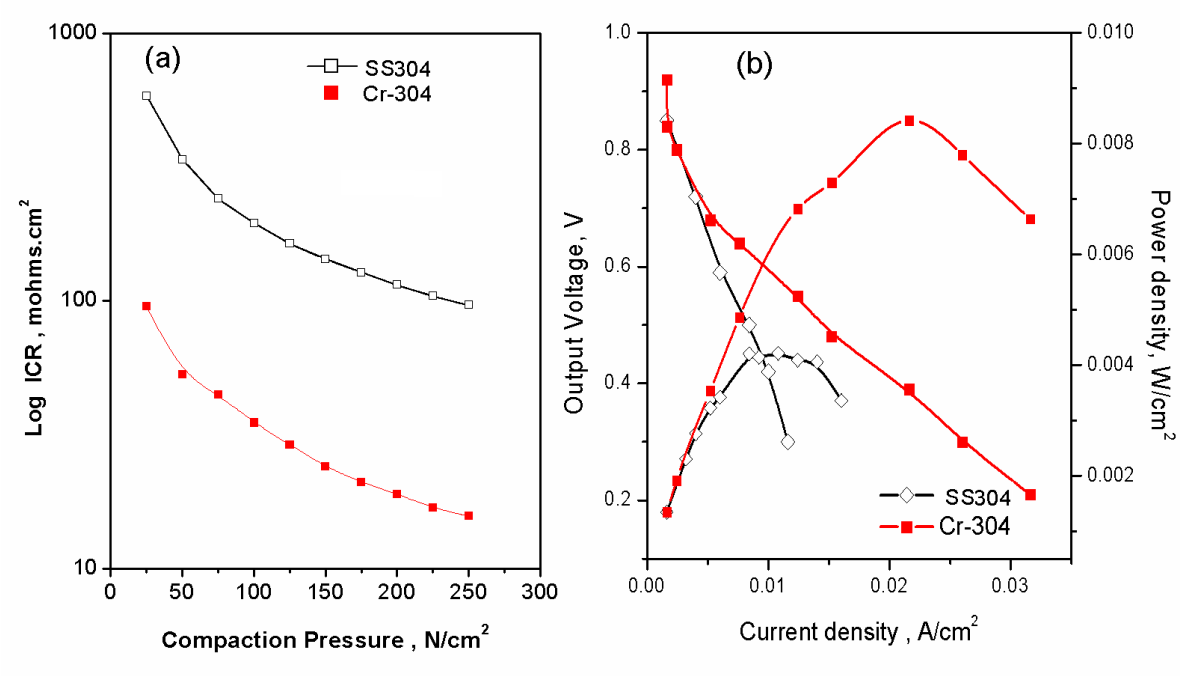

Fig. 7: (a) Plot of ICR against compaction pressure for Cr-304 and SS304 (b) Single fuel cell performance of Cr-304 and 304SS bipolar plates.

The initial polarisation of the single cells assembled with 304 stainless steel coated (Cr-304) and uncoated (SS304) with the optimised process parameters is shown in Fig. 7b. The cell with Cr-304 bipolar plates had an open circuit potential (OCP) was 0.92 V while that for SS304 was 0.85 V. As current density increased, the beneficial influence of the chromised coatings becomes evident as the voltage of SS304 decreased rapidly compared to that of the coated plates. As shown in Table 6, the single cell with Cr-304 bipolar plates attained a maximum power density of 8.47 mW/cm^2 at a current density of 21.60 mA/cm^2. These results represent a two-fold increase in the maximum power density of the single fuel cell with SS304 bipolar plates and suggest that chromised stainless steels produced without pre-

treatments can be considered for bipolar plate application. Comparison of the ex-situ ICR values of Cr-304 and SS304 with the single fuel cell performance of these materials shown in Table 6 indicates that the performance of the single fuel cells was consistent with the ICR values at the compaction pressures at which the cells were assembled (Table 6); hence, the higher power output of the cell with Cr-304 bipolar plate than that the cell with SS304 bipolar plate. This observation is in agreement with the literatures on single fuel cell performance [8, 10].

4.0 Conclusion.

The influence of time, activator content and temperature on the corrosion current density of pack-chromised 304 stainless steel in simulated PEMFC environment of 0.5M H_2SO_4 + 2 ppm HF at 70^oC was systemically investigated using Box–Behnken design. The results showed that corrosion current density decreased parabolically with temperature and increased linearly with time while the influence of the activator content was negligible. Nevertheless, the interaction between the temperature and activator content was found to be statistically significant. The coating produced at the optimised process conditions exhibited about an order of magnitude decrease in the corrosion current density and contact resistance of the substrate in the compaction pressure range of interest for PEMFC applications. Consequently, the single fuel cell with chromised 304 stainless steel bipolar plates outperformed the cell assembled with uncoated 304SS having a voltage of 0.92 V at open circuit condition and maximum power density of 8.42 mV at current density of 21.60 mA. The improvement in performance of the optimised chromised 304 stainless steel over that of the uncoated steel in both the ex-situ and in-situ environments was attributed to the presence

of chromium carbides and nitrides on the near surface of the optimised chromised 304 stainless steel.

5.0 References

1. O. Z. Sharaf, M. F. Orhan, An overview of fuel cell technology: fundamentals and applications, Renewable and Sustainable Energy Reviews 32 (2014); 810- 853.
2. H-W Wu, A review of recent development: Transport and performance modelling of PEM fuel cells , Applied Energy 165 (2016) 81–106
3. M.P. Brady, H. Wang, J.A. Turner, H.M. Meyer III, K.L. More, P.F. Tortorelli, B.D. McCarthy, Pre-oxidized and nitrided stainless steel alloy foil for proton exchange membrane fuel cell bipolar plates: Part 1. Corrosion, Interfacial contact resistance, and surface structure, J. Power sources, 195 (2010) 5610 -5618.
4. J.G. Carton, A.G. Olabi, Energy, Design of experiment study of the parameters that affect performance of three flow plate configurations of a proton exchange membrane fuel cell, Energy 35 (2010) 2796-2806
5. A. M. Oladoye, J. G. Carton, and A. G. Olabi, Evaluation of CoBlast Coated Titanium Alloy as Proton Exchange Membrane Fuel Cell Bipolar Plates J. Materials, vol. 2014, Article ID 914817, 10 pages, 2014. doi:10.1155/2014/914817.
6. M. Brady, B. Yang, H. Wang, J. Turner, K. More, M. Wilson, F. Garzon ,The formation of protective nitride surfaces for PEM fuel cell metallic bipolar plates, JOM 58 (8) (2006), 50-57.
7. H. Wang, M.A. Sweikart, J.A. Turner, Stainless steel as bipolar plate material for polymer electrolyte membrane fuel cells, J. Power Source, 115 (2) (2003) 243-251.

8. K. Feng, G. Wu, T. Hu, Z. Li, X. Cai, P. K. Chu, Dual Ti and C ion-implanted stainless steel bipolar plates in polymer electrolyte membrane fuel cells, Surf. Coat Technol. 206 (2012) 2914–2921.
9. Y. Show, Electrically conductive amorphous carbon coating on metal bipolar plates for PEFC, Surf. Coat Technol., 202 (2007), 1252-1255.
10. P. Yi, L. Peng, L. Feng, P. Gan, X. Lai, Performance of a proton exchange membrane fuel cell stack using conductive amorphous carbon-coated 304 stainless steel bipolar plates, J. Power Sources 2010; 195(20): 7061-7066.
11. K.H. Cho, W.G. Lee, S.B. Lee, H. Jang, Corrosion resistance of chromized 316L stainless steel for PEMFC bipolar plates, J. Power Sources 178 (2008) 671–676.
12. S.B. Lee, K.H. Cho, W.G. Lee, H. Jang, Improved corrosion resistance and interfacial contact resistance of 316L stainless-steel for proton exchange membrane fuel cell bipolar plates by chromizing surface treatment, J. Power Sources 187 (2009) 318–323.
13. L. Yang, H. Yu, L. Jiang, L. Zhu, X. Jian, Z. Wang, Improved anticorrosion properties and electrical conductivity of 316L stainless steel as bipolar plate for PEM fuel cell by lower temperature chromizing treatment, J. Power Sources 195 (2010) 2810–2814.
14. T-M. Wen , K-H Hou , C-Yuan Bai , M-Der Ger , P-H Chien , S-J Lee, Corrosion behaviour and characteristics of reforming chromized coatings on SS 420 steel in the simulated environment of proton exchange membrane fuel cells, Corros. Sci. 52 (2010) 3599–3608.
15. C-Y. Bai, T-M Wen, M-S Huang, K-H Hou, M-D Ger, S-J Lee, Surface modification and performance of inexpensive Fe-based bipolar plates for proton exchange membrane fuel cells, J. Power Sources 195 (2010) 5686–5691.
16. D.C. Montgomery, Design and analysis of experiments, John Wiley &Sons Inc 2013.

17. C. Saikaew, A. Wisitsoraat, R. Sootticoon Optimization of carbon doped molybdenum oxide thin film coating process using designed experiments, Surf. Coat Technol. 204 (2010) 1493–1502.
18. O. Keles, G. Aykac, O. T. Inal, The role of parameter in plasma assisted vapour deposition of tin/tin oxide coatings, Surf. Coat Technol. 72 (2003), 166-175.
19. N. Lin, F. Xie, T. Zhong, X. WU , W.Tian, influence of process parameters on thickness and wear resistance of rare earth modified chromium coatings on P110 steel synthesized by pack cementation, J. Rare Earths 28, (2010), 301-304.
20. Z.B. Wang, J. Lu, K. Lu, Wear and corrosion properties of a low carbon steel processed by means of SMAT followed by lower temperature chromizing treatment, Surf. & Coat. Technol. 201 (2006) 2796–2801.
21. K.D. Ralston, D. Fabijanic, R.T. Jones, N. Birbilis, Achieving a chromium rich surface upon steels via FBR-CVD chromising treatments, Corro. Sci. 53 (9) (2011) 2835–2842.
22. J. Creus, H. Mazille, H. Idrissi, Porosity evaluation of protective coatings onto steel, through electrochemical techniques, Surf. Coat. Technol. 130 (2000) 224-232.
23. R. Bianco, R.A. Rapp. Pack Cementation Diffusion Coatings, Metallurgical and Ceramic Protective Coatings (1996), 236–260.
24. N. Tabet, I. Allam, R.C, Yin, X-ray photoelectron spectroscopy investigation of the carburization of 310 stainless steel , Applied Surf. Sci. 195 (2002) 166–174.
25. M. Detroye, F. Reniers, C. Buess-Herman, J. Vereecken, AES–XPS study of chromium carbides and chromium iron carbides, Applied Surf. Sci. 144–145 (1999) 78–82.
26. A. Lippitz, T. Hubert, XPS investigations of chromium nitride thin films, Surf. Coat. Technol. 200 (2005) 250 – 253.

27. A. Conde, A.B. Cristóbal, G. Fuentes, T. Tate, J. de Damborenea, Surface analysis of electrochemically stripped CrN coatings, Surf. Coat Technol., 201 (2006) 3588-3595.
28. L. Wang, J. Sun, B. Kang, S. Li, S. Ji, Z. Wen, X. Wang Electrochemical behaviour and surface conductivity of niobium carbide-modified austenitic stainless steel bipolar plate J. Power Sources, 246 (2014) 775-782.
29. M.S. Ismail, T. Damjanovic, D.B. Ingham, M. Pourkashanian, A. Westwood, Effect of polytetrafluoroethylene-treatment and microporous layer-coating on the electrical conductivity of gas diffusion layers used in proton exchange membrane fuel cells, J. Power sources 195 (2010) 2700–2708.
30. A. El-kharouf, T. J. Mason, Dan J.L. Brett, Bruno G. Pollet, Ex-situ characterisation of gas diffusion layers for proton exchange membrane fuel cells, J. Power sources 218 (2012) 393–404.

6.0 Appendix

Appendix A, B and C can be found in the supplementary material.